A feasability study of limitations on the creation of microscopic black holes at the LHC using the hydrogen atom.

Jins de Jong

07-27-2009

Chapter 1

The LHC threats

The Large Hadron Collider (LHC) is a particle accelerator at the Conseil Européen pour la Recherche Nucléaire (CERN). The collisions it produces will reach energies of 14 TeV, which is a new record. With these high energies unknown physics can be explored. Because physicists are unfamiliar with such high energies, in principal it is not known what will happen.
Very soon after commencing the building of the LHC various theories arose claiming the destruction of the Earth due to collision experiments. As a result of internet broadcasting, newspaper headlines and books predicting the destruction of the Earth when the LHC was tested, lawsuits and even suicide occurred around the world. Although in the autumn of 2008 the first beams circled beneath Swiss and France, no high energy collision has taken place yet, which gives us the time to have a final look at the safety.

The theories proposed are not generally accepted and most of them can be firmly rejected, but, prior to that, have to be taken seriously. Without any doubt the major fear concerns the creation of a microscopic black hole. Another doom scenario is the creation of exotic, hypothetical particles called 'strangelets'. Furthermore, a magnetic monopole could be created. The last option is the creation of a vacuumbubble.

In the remaining part of this chapter we will discuss these theories more in depth and provide arguments to reject them. The most powerful tool to do that is the so called 'Cosmic ray argument', which will be introduced first.

1.1 Cosmic ray argument

Since the first particle accelerators in the early thirties the operating energies of these accelerators have increased from 1 MeV to 7 TeV in the near future at the LHC. However, this is still miles away from the energies reached around us by cosmic rays, mostly protons, striking the atmosphere, which go up to 10^{20} eV. The Earth exists about 4.5 billion years now and all these years Earth has been bombarded by these cosmic rays. After all these 'experiments' no trace is found of an event that could lead to Earth's destruction.
A cosmic proton hitting the Earth's atmosphere with 10^{17} eV is comparable with a full speed collission at CERN. The flux of such particles is about 10^5 per second, leading to 10^{22} cosmic ray collisions in Earth's history. This corresponds with a hundred thousand full length LHC experiments [7].
As far as we know all of the visible objects in the universe are subject to cosmic rays and none of them reveal a severe consequence of these cosmic rays, nor do we find any remains of astrophysical objects that are destroyed as a result of cosmic particles smashing upon it. Considering this, already many of the above stated threats which might occur at the LHC are ruled out. The white dwarf is of special interest to us, because it is very long-lived and does not seem to disappear, so that we can state that cosmic rays on white dwarfs do not cause its destruction. The particle and mass densities of white dwarfs are enormous, so that any crossing object has a relatively high chance of interacting with the white dwarf. Furthermore, heavy products of cosmic ray collisions

are very much attracted gravitationally to the white dwarf as a result of its high mass density and may very well get trapped inside a white dwarf.
However, there is one significant difference between the collisions at the LHC and in the atmosphere: at the LHC two beams move towards each other, while in the atmosphere a very fast particle strikes a particle at rest. Since the only relevant energy in a collision is the centre of mass energy, this difference leads to a lower centre of mass energy and a large final momentum of the particles for collisions in space. Comparable collisions have the same centre of mass energy and therefore cosmic ray collisions comparable with LHC collisions have much higher energies (when measured on Earth), since the total momentum is not zero. This difference between LHC collisions and cosmic ray collisions must be considered carefully when we use this argument.

1.2 Vacuumbubbles

For more than 25 years theories have been known concerning the (meta)stability of the universe that we know [8]. 'Our' vacuum might not be the stable state having the lowest energy, but separated by huge potential walls from the absolute minimum. The time expected for a 'vacuum decay' to occur is more than the age of the universe, because any such decay has not happened yet. At high energy particle collisions there could be an enhanced probability for such a decay, leading to a small vacuumbubble. Such a bubble would expand with approximately the speed of light, consuming Earth and the near universe soon afterwards.
As stated in section 1.1, already a hundred thousand equivalents of a full LHC experiment have been conducted on the Earth's atmosphere and no sign of a vacuumbubble has been observed. The same conclusions can be drawn for other visible objects around us. This leads us to the conclusion that there is no threat from vacuumbubbles when turning on the LHC.

1.3 Magnetic monopoles

Magnetic monopoles are speculative, just like the vacuum bubbles. However, there is one difference. Magnetic monopoles serve a greater good, since only one monopole would be enough to explain the quantization of all electric charge in the universe. It can be shown that for the product of the magnetic charge g and the electric charge e the following equation must hold [5]:

$$e \cdot g = \frac{1}{2} n\hbar \qquad n \in \mathbb{N} = \{1, 2, \ldots\} \qquad ,$$

with $\hbar$ the reduced Planck constant. Because of the difference in magnitude between e and $\hbar$ this implies a large magnetic charge. Grand unified theories predict that a magnetic monopole could cause nucleon decay, which would harm the Earth severely. However, such monopoles are expected to have masses of at least 10^{15} GeV [7], exceeding the available energy at the LHC. We can state independently of this that if a magnetic monopole could be created by the LHC, then many of them would already have been made by cosmic rays. But then white dwarfs would be bombarded with many magnetic monopoles, which would lead to the white dwarf's destruction. Since this has not been observed we conclude that magnetic monopoles are no real disaster scenario for the Earth.

1.4 Strangelets

Strangelets are lumps of up, down and strange quarks. They are proposed as a threat for the Earth's existence.
The Pauli-exclusion principle prohibits identical quarks to be in the same quantum state. If there are a large number of up and down quarks in such an environment they all have to occupy a different quantum state. The energy corresponding to the highest quantum state may be large enough to create a heavier strange quark. This strange quark can occupy a low energy state, since it's a different particle. In this situation it would be energetically favourable to convert down quarks to strange quarks and in very large strangelets the number of up, down and strange quarks would become comparable.

To create strangelets one clearly looks at places with relatively high numbers of quarks. Heavy-ion collisions at the LHC are designed to create quark-gluon plasmas with a lot of energetic quarks. The way strangelets might form a safety hazard is that they are supposed to convert normal matter to strange matter, leading to an ever growing strangelet. No exact theory prediction exists, since we are not able to calculate with Quantum Chromo Dynamics (QCD) what will happen. Any calculations on strangelet production are done using simplifying models, like the 'bag model' [2]. Using the bag model it is shown that strangelet production at the LHC is more unlikely than at the Relativistic Heavy Ion Collider (RHIC) [7], which operates at Brookhaven National Laboratory (BNL) and where no strangelet production is observed. Independently of this, we can exclude any danger from strangelets by using experimental facts.
Due to the relatively low density of heavy atoms in the atmosphere more stringent limits are found by studying objects without atmosphere, since collisions there take place in a high density environment. The moon, for example, has been subject to cosmic rays as long as it exists, and has a crust that consists mainly of metals. Cosmic rays contain abundances of heavy atoms as well and colliding with the moon this simulates a heavy-ion collision. As a result of these cosmic rays the moon should have been converted to strange matter, which it has not.
Stronger limits are obtained by observing so called 'killer astroids' [4], [9]. If continually growing strangelets exist, there should be astroids converted to strange matter due to a cosmic ray while they were flying through space. When such killer astroids crash upon a star they convert it to strange matter entirely, which would be observable. The limits these processes generate are very reassuring and we may conclude that strangelets are no threat.

1.5 Microscopic black hole disaster scenario

A black hole may be viewed upon as a volume of space that contains so much energy that the escape velocity exceeds the speed of light. The boundary of this volume is called the Schwarzschild radius, which is the radius where the escape velocity matches the speed of light.[1]
This means that it is classically not possible for anything to escape from a black hole. However, quantum mechanically it is possible for a black hole to radiate by Hawking radiation. In a simplified picture Hawking radiation can be described as the creation of a pair of a particle and its antiparticle due to quantum fluctuations near the Schwarzschild radius. One of these particles is attracted towards the centre of the black hole and the other can be blown into space. This particle can be observed far away from the black hole, so that the black hole effectively radiates and loses energy. Calculations show that the emitted power increases with decreasing mass [10].
If black holes could be made at the LHC, we would expect them to decay almost immediately, because of this Hawking radiation. However, since it has never been identified experimentally, Hawking radiation might be much weaker or not exist at all. This however does not mean that black holes will be dangerous.
If the LHC could make them, also cosmic rays bombarding white dwarfs should have made many black holes. These black holes could become trapped gravitationally in a white dwarf, which would lead to the white dwarf's end. Furthermore, a black hole accreting a white dwarf is expected to emit intense light, which would be observable. However, no destruction of a white dwarf has been observed. This leads to two possibilities. The first is that no black holes will be made by cosmic rays, so that no black holes will be made by the LHC.
The second option is that the white dwarf accretion by the black hole takes longer than the age of the universe to lead to observable effects, since white dwarfs are long-lived. That leads us to the conclusion that if black holes can be made we expect them either to decay very soon or accrete matter very slowly.

Now we have argued that all popular doom scenarios for the Earth will not occur, so that we can safely conduct experiments with the LHC.
Although we know that black holes will not destroy the Earth, we are not entirely certain if they can be made at the LHC. If it would be possible to make black holes in a controlled environment

[1] We do not take into account more complicated black holes, like rotating or charged black holes.

Hawking radiation may be tested. Also experiments on quantum gravity may be conducted, since this would be the first known system that behaves quantum mechanically in which gravity definitely may not be neglected. This is a very exciting possibility, which would lead to much new physics.

In the rest of this thesis we will study if it is possible for harmless microscopic black holes to be made at the LHC. In chapter 2 we will construct spaces that may allow black hole creation at the LHC and calculate the gravitational effects. In chapter 3 we will use these results to see if black hole creation is ruled out by atomic physics.

Chapter 2

Submillimeter gravitation

Today classical Newtonian gravity has been tested down to scales of tens of microns [1]. Below these distances not much is known about gravity, although somewhere quantum gravity must be taken into account. Unfortunately, no theory of quantum gravity exists, so we will operate classically.

To see how long we can safely operate classically we define the Planck length l_P as the unique length that can be constructed from the speed of light c, the reduced Planck constant $\hbar$ and Newtons constant G_N:

$$l_P = \sqrt{\frac{\hbar G_N}{c^3}} = 1,62 \cdot 10^{-35} \text{ m} \tag{2.1}$$

To see that this is the scale at which we must include quantum gravity we conduct the following thought experiment. Suppose we use a photon to measure the position of a particle with an uncertainty smaller than the Planck length. The uncertainty in the momentum Δp then becomes

$$\Delta p \geq \frac{1}{2}\sqrt{\frac{\hbar c^3}{G_N}} \quad ,$$

which corresponds with a large uncertainty in the energy $\Delta E = c \cdot \Delta p$. The photon has enough energy to create a particle with half a Planck mass m_P, which is defined in the same fashion as the Planck length:

$$m_P = \sqrt{\frac{\hbar c}{G_N}} \quad .$$

This particle has a Schwarzschild radius

$$r_S = \frac{2G_N \frac{1}{2} m_P}{c^2} = l_P \quad .$$

This means that when studying objects at the Planck scale we have to include quantum gravity, since a black hole with the size of our system appears naturally when doing quantum mechanics at this scale. To create black holes at the LHC the Planck length should coincide with the length scale of the LHC, which is just below the attometer (10^{-18} m). This means that gravity has to increase at small scales compared to Newtonian gravity, since we see using equation (2.1) that $l_P \ll l_{LHC}$ [7]. A proposed scenario [3] is that there may be relatively small extra dimensions increasing the gravitational force at small distances.

In this chapter we will calculate the gravitational consequences of such extra dimensions. Using the results from this chapter we subsequently try to restrict the possibilities using atomic physics and see what consequences this has for the creation of black holes at the LHC.

2.1 Strong gravity

In agreement with classical gravity we will assume that gravity is a classical field theory. This means that the force $\vec{F}$ a particle experiences matches the flux it absorbes and that the total amount of flux Φ is conserved. If we integrate over a closed surface with an orientation $\overrightarrow{dA}$ of a volume V we have

$$\Phi = \oint_{\partial V} \overrightarrow{\mathrm{d}A} \cdot \vec{F} \quad \Rightarrow \quad \vec{F} = -\frac{d\Phi}{dA}\,\hat{r} \qquad , \tag{2.2}$$

where the minus sign accounts for the attractive direction $-\hat{r}$ of the force, ∂V denotes the surface of the volume and $d\overrightarrow{A}$ is an infinitesimal orientated surface element.

The force is obtained by spreading the gravitational flux K over a three-dimensional sphere. With m_1 and m_2 two test masses, choosing $K = 4\pi G_N m_1 m_2$ yields Newton's gravitational law:

$$F = \|\vec{F}\| = \frac{K}{4\pi r^2} \quad \text{with} \quad K = 4\pi G_N m_1 m_2 \Rightarrow F = \frac{G_N m_1 m_2}{r^2}$$

In the standard Newtonian case gravity is too weak for microscopic black holes to be made at the LHC. So, let us add n extra dimensions and see what happens.
As in a three-dimensional world, also in an $(n+3)$-dimensional world the gravitational flux is conserved. The surface of an $(n+3)$-dimensional volume is an $(n+2)$-dimensional surface. From the conservation of flux the length dependent part of the force law is obtained. When we define the other part as $G_N^{(n)} m_1 m_2$, where $G_N^{(n)}$ is the higher-dimensional gravitational constant, it follows from equation 2.2 that

$$\Phi = \oint \mathrm{d}\vec{A} \cdot \vec{F} \quad \Rightarrow \quad F = G_N^{(n)} m_1 m_2 \frac{1}{r^{D-1}} \quad , \tag{2.3}$$

where D is the number of spatial dimensions.
This implies that gravity increases much faster than expected from Newton's law.

We can now read off what consequences this has for the Planck scale. We can see from a dimensional analysis that $\left[G_N^{(n)}\right] = L^n \left[G_N\right]$ with L some quantity with the dimension of length. Using equation 2.1 we see that $\left[G_N^{(n)}\right] = L^{2+n} \left[c\right]^3 \left[\hbar\right]^{-1}$. Since the Planck length is the unique length scale constructable from c, $\hbar$ and the gravitational constant $G_N^{(n)}$, we obtain for the Planck scale in our space with n added dimensions

$$\left(l_P^{(n)}\right)^{2+n} = \left(l_P\right)^2 \frac{G_N^{(n)}}{G_N} \quad . \tag{2.4}$$

For more precise formulas the actual compactifications of space is required. An example of this can be found at the end of this chapter. Following the same steps as before we find that this modified Planck length $l_P^{(n)}$ is the Schwarzschild radius of a particle with half the Planck mass m_P, using the higher-dimensional Schwarzschild radius for an object with mass M:

$$r_S = \left(\frac{2G_N^{(n)} M}{c^2}\right)^{\frac{1}{1+n}}$$

This means that the modified Planck length is still the length scale we expect quantum gravity to become important.

2.1.1 Differences with other forces

We know four forces building up the universe, of which the gravitational and electromagnetic force are two examples. Newton's gravitational law and Coulomb's electrostatic law are two classical expressions for these forces.

One might wonder why Coulomb's law does not increase at small distances. This is much easier to verify and has not been observed. Coulomb's law falls off with $\frac{1}{r^2}$ as well and seems to do this all the way down to the electroweak length scale, $l_\omega = 10^{-18}$ m.
At least for now, the answer is hypothetic. Suppose that the graviton carries the gravitational force, just like the photon carries the electromagnetic force. If there exist some extra dimensions through which the photon cannot propagate but the graviton can, Coulomb's law will not change, but Newton's law can [6].
There are no obstructions to this hypothesis right now, as long as we demand that at macroscopic lengths Newton's law is again recovered.

2.2 Compact submillimeter dimensions

We assume that we have a space with 'small extra dimensions'. How can a dimension become invisible and why does it look like $\mathbb{R}^3$ at 'large scales'? Imagine a high-voltage cable. For a human in a meadow staring at the cable it looks like a one-dimensional string. An insulated bug walking on the cable sees it as a two-dimensional surface. A similar mechanism works for a three-dimensional space.
In the above example we added one dimension, but of course more dimensions and more constructions may be possible. We have neither a limit for the number of extra dimensions, nor for the size of the dimensions. This makes it hard to handle and therefore we make a few assumptions.
The first is that we will only add spherical dimensions S^1, because in this way it is possible to calculate many things explicitly and fairly easily. Since these extra dimensions are spherical they should have a radius, in this case also referred to as the size of the extra dimension. This radius is called the 'crossover radius' R_C. For different dimensions there may be different crossover radii, often denoted by $R_1, R_2, \ldots, R_n$. At distances much larger than the crossover radius the extra dimension is not visible or experienced, so that submillimeter dimensions will not change daily life. At or below this radius gravity increases much faster than expected from Newton's law.
The second assumption we make is that we will assume sometimes that all the crossover radii are the same. Sometimes we want to limit the number of extra dimensions, so we do not want to have to include every configuration of sizes possible. Then this assumption makes our equations easier and restricts the number of parameters. The following reasoning explains why we are allowed to do so.
If we study gravity at a certain scale we can ignore any dimension with a size significantly smaller than that scale, since it cannot be observed at that scale yet.
The way we will restrict the possibilities is by calculating the effects of adding dimensions on the energy levels of the hydrogen atom. A stronger gravitational force gives a higher potential difference as compared to the system without added dimensions. A higher potential difference is easier to measure.
Consider a gravitational experiment at a certain length scale. Taking all crossover radii the same, we will find that for R_C equal to the length scale of the experiment there is a maximum number of extra dimensions n that cannot be excluded by the present data. If one of the dimensions would have a significantly larger size, the potential difference would increase, resulting in a larger extra dimensional effect. So the limits that we obtain are conservative. Dimensions with significantly smaller sizes should not be counted, since they have no effects at this scale.

2.3 $\mathbb{R} \times S^1$

Using the concepts and the assumptions from the previous paragraph we can see what it results in for a fairly easy space. We take a one-dimensional space $\mathbb{R}$ and one added dimension S^1 with crossover radius R_C. This yields, visualized in three dimensions, the cylinder in figure 2.1.
In $\mathbb{R}^3$ the distance between two points is determined by the length of the straight line connecting the two points. On a cylinder there are many straight lines from one point to another, since the cylinder is periodic, and each of these lines has its own length.

When we look how this relates to gravity we notice that in $\mathbb{R}^3$ the force is determined by the length of the straight line connecting the two masses and that the force is directed along that straight line. On this cylinder we have many straight lines between the two masses and they all contribute to the total force. Each line corresponds to a contribution to the force with its strength determined by the length of the line and its direction by the direction of the line. The total force now is simply obtained by summing all these lines.

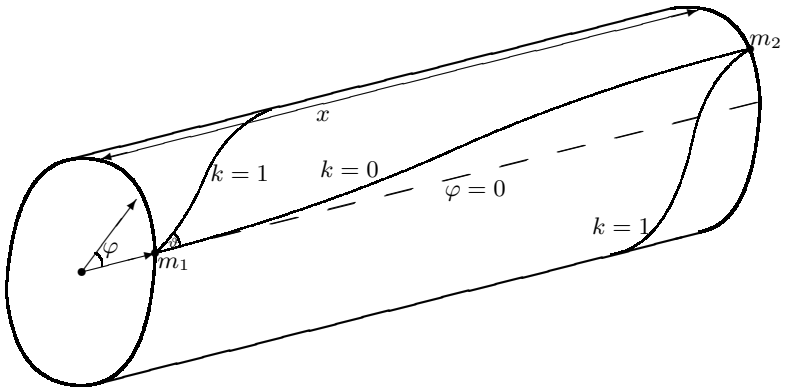

Figure 2.1: $S^1 \times \mathbb{R}$ visualized in three dimenions.

Because we want to make this quantitative we need coordinates (x, φ), with $\varphi \in (-\pi, -\pi]$ the circular coordinate and $x \in \mathbb{R}$ the translational coordinate, and we place two masses m_1 and m_2 on the surface of our cylinder. Due to the rotational symmetry around the cylinder axis it is only the difference in φ that matters and we are allowed to put m_1 at $(x = 0, \varphi = 0)$ and m_2 at $(x > 0, \varphi)$. To see what the straight lines are on the cylinder we unfold it (figure 2.2). This shows that the trajectories with $\ddot{\varphi} = 0$ and $\ddot{x} = 0$ are indeed straight lines.

Since we want to know the force we need to sum all the straight lines from m_1 to m_2. These lines can be labeled by k, the number of revolutions a line makes. The $(k = 1)$-line is drawn in figure 2.1. Finally, the surface of the cylinder is two-dimensional, so that all straight lines emanating from m_1 can be parametrized by one angle $\vartheta \in (-\pi, \pi]$, since we have only one line per direction. The angle ϑ fixes the direction of the force contribution belonging to a specific line. The lengths of the lines determine the corresponding strengths. The total force is obtained by summing all force vectors.

In a two-dimensional space a surface is a one-dimensional line. We will assume that at m_1 the space is isotropic, i.e. locally the directions $\hat{x}$ and $R_C\,\hat{\varphi}$ are equivalent. This means that at small scales the space looks two-dimensional.
The flux in the narrow band $(\vartheta, \vartheta + d\vartheta)$ at unity from m_1 is $\frac{K}{2\pi} \mathrm{d}\vartheta$, because the total flux is conserved and spread equally over all directions. The force on m_2 in the direction $-\hat{\lambda}(\vartheta)$ defined by one of

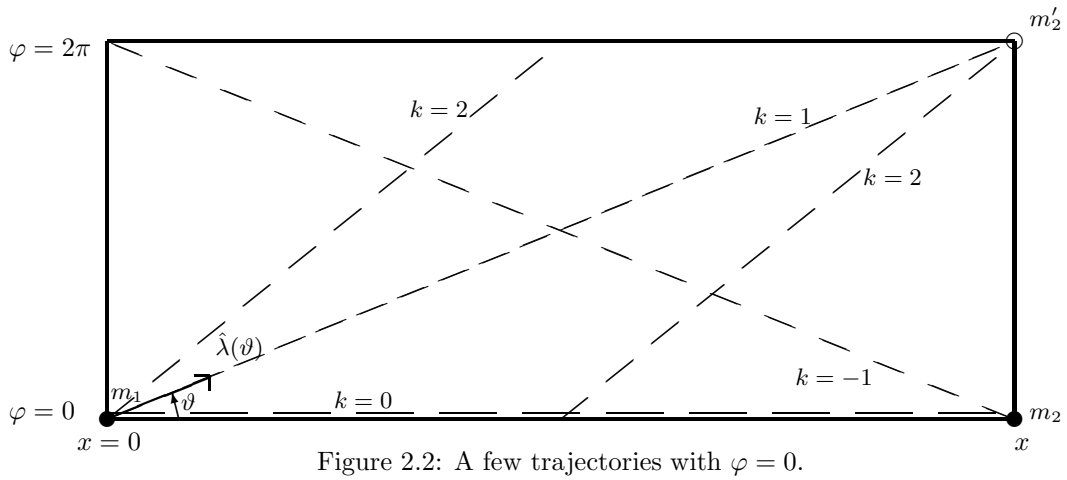

Figure 2.2: A few trajectories with $\varphi = 0$.

Note that m_2' is a mirror image of m_2. Furthermore, the interval $(-\pi, \pi]$ has been shifted to $(0, 2\pi]$.

the straight lines around the cylinder with length L becomes

$$F_{-\hat{\lambda}(\vartheta)}(\vartheta) = \frac{\mathrm{d}\Phi}{\mathrm{d}A} = \frac{\frac{K}{2\pi}\mathrm{d}\vartheta}{L(\vartheta)\mathrm{d}\vartheta} = \frac{K}{2\pi L(\vartheta)} \quad , \tag{2.5}$$

with $\hat{\lambda}(\vartheta)$ the unit vector along the straight line from m_1 to m_2 with an angle ϑ with respect to the positive x-direction. We separate $\mathbb{R} \times S^1$ according to the different behaviour of the two parts: the extended translational part and the periodic part. For every line we define its angle with respect to the positive x-direction by:

$$\tan(\vartheta) \equiv \frac{(2\pi k + \varphi)R_C}{x} \quad \Rightarrow \quad \vartheta = \arctan(\frac{(2\pi k + \varphi)R_C}{x}) \quad . \tag{2.6}$$

With this equation the travelled length becomes

$$L = \sqrt{x^2 + R_C^2(2\pi k + \varphi)^2} = \frac{x}{\cos(\vartheta)} \tag{2.7}$$

and the total force

$$\vec{F} = \frac{K}{2\pi} \sum_{k \in \mathbb{Z}} \frac{-\hat{\lambda}(\vartheta)}{\sqrt{x^2 + R_C^2(2\pi k + \varphi)^2}} \quad . \tag{2.8}$$

Note that the values for which $\cos(\vartheta) < 0$ correspond with negative x, so that L remains positive. We only use positive x and therefore $\vartheta \in (-\frac{\pi}{2}, \frac{\pi}{2})$. The negative part of this interval is for the part with negative k. We could have defined ϑ positive, but then we would have needed an additional variable to account for the direction of the force.

2.3.1 Macroscopic limit

Since we expect this space to behave one-dimensional macroscopically, only the x-component should remain in the macroscopic limit. This is why we are more interested in the x-component. Using equations 2.7 and 2.8 we find for the x-component of the total force:

$$F_{-\hat{x}} = \frac{K}{2\pi} \sum_{k \in \mathbb{Z}} \frac{\cos^2(\arctan(\frac{(2\pi k + \varphi)R_C}{x}))}{x} \tag{2.9}$$

From equation 2.3 we know that flux conservation requires gravity to fall off with r^{1-D}. Since $\mathbb{R} \times S^1$ behaves one-dimensional at large scales we expect that gravity becomes constant, i.e. equation 2.8 should in the limit $\frac{x}{R_C} \to \infty$ converge to a constant.

For $\frac{x}{R_C} \to \infty$, the angle between the k- and $(k+1)$-line is very small and the sum from equation 2.9 becomes an integral:

$$F_{-\hat{x}} = \sum_{k\in\mathbb{Z}} \frac{K}{2\pi R_C} \cos^2(\arctan(\frac{(2\pi k+\varphi)R_C}{x})) \left(\frac{(k+1)R_C}{x} - \frac{kR_C}{x}\right) \quad \Rightarrow$$

$$\lim_{\frac{x}{R_C}\to\infty} F_{-\hat{x}} = \int_{-\infty}^{\infty} \frac{K}{2\pi R_C} \cos^2(\arctan(\frac{(2\pi k+\varphi)R_C}{x}))\mathrm{d}\frac{R_C k}{x}$$

This is a Riemann integral, which we can easily solve now using equation 2.6:

$$\lim_{\frac{x}{R_C}\to\infty} F_{-\hat{x}} = \frac{K}{2\pi R_C} \int_{-\frac{\pi}{2}}^{\frac{\pi}{2}} \mathrm{d}\vartheta \cos^2(\vartheta) \frac{R_C}{x}\frac{dk}{d\vartheta} = \frac{K}{4\pi^2 R_C} \int_{-\frac{\pi}{2}}^{\frac{\pi}{2}} \mathrm{d}\vartheta = \frac{K}{4\pi R_C} \tag{2.10}$$

Indeed, this becomes a constant.

For the φ-component of $F_{-\hat{\lambda}(\vartheta)}(\vartheta)$ we obtain

$$F_{-\hat{\varphi}}(\vartheta) = F_{-\hat{x}}(\vartheta)\tan(\vartheta) \Rightarrow F_{\hat{\varphi}} = \frac{K}{4\pi^2 R_C} \int_{-\frac{\pi}{2}}^{\frac{\pi}{2}} \tan(\vartheta)\mathrm{d}\vartheta = 0$$

Equation 2.10 is not only the expression for the x-component of the gravitational force, it is the expression for $\vec{F}$ as well.

2.3.2 Microscopic limit

At small scales the x and φ-directions are equivalent and it would be surprising if there were any effects due to the shape of the space macroscopically. Thus we expect gravity to decrease like r^{-1}. Let the two masses be separated by a vector $\vec{\lambda}$ that points in both the extended dimension $\mathbb{R}$ and the extra dimension S^1. The distance has to be small compared to the length scale of the cylinder R_C, so that $\frac{\|\vec{\lambda}\|}{R_C} \longrightarrow 0$. Then $x^2 \ll R_C^2(2\pi k+\varphi)^2$, if $k \neq 0$. Neglecting x^2, we compare the $(k=0)$-term with all the $(k\neq 0)$-terms from equation 2.8:

$$\lim_{\frac{\|\vec{\lambda}\|}{R_C}\to 0} \left\| \frac{\sum_{k=1}^{\infty} \frac{K}{2\pi}\left(\frac{1}{R_C(2\pi k+\varphi)} + \frac{1}{R_C(-2\pi k+\varphi)}\right)}{\frac{K}{2\pi}\frac{1}{\|\vec{\lambda}\|}} \right\| = \lim_{\frac{\|\vec{\lambda}\|}{R_C}\to 0} \left\| \frac{\|\vec{\lambda}\|}{R_C} \sum_{k\in\mathbb{N}} \frac{2\varphi}{\varphi^2 - 4\pi^2 k^2} \right\| = 0 \tag{2.11}$$

In the microscopic limit only the $(k=0)$-term contributes, which leads to the expected behaviour:

$$\vec{F} = \frac{K}{2\pi} \frac{-\hat{\lambda}(\vartheta)}{\sqrt{R_C^2\varphi^2 + x^2}} \tag{2.12}$$

2.4 The easier way

Now that the results for the easiest case are obtained it is time to wonder how practical this way of computing is. That is a relevant question, since the goal is to be able to make some statements about the behaviour of gravity at small scales. In the above case everything was easy to imagine and the number of variables was limited. However, for more than one added dimension it is not possible to visualize this space in three-dimensions anymore and the equations will not get prettier either.

These problems can be solved using the following construction: for p extended dimensions and n extra compact dimensions we use $\mathbb{R}^{p+n}$. Instead of a periodic dimension we now have an infinite axis that describes how much a straight line has travelled in the extra dimension. By doing this we construct a space in which all the straight lines on the cylinder from paragraph 2.3 are straight lines in $\mathbb{R}^{(p+n)}$ as well.
We gave up the geometrical point of view, but in return we got a space where all straight lines are

nicely distributed in a n-dimensional subspace. Since we did not change the lengths in the extended translational and extra dimensions our angle ϑ from equation 2.6 is the same. Furthermore, notice that the space around m_1 has not changed. It was flat and $(p+n)$-dimensional and it still is. For $\mathbb{R} \times S^1 \times S^1$ the obtained space looks like figure 2.4.

2.4.1 $\mathbb{R} \times S^1$

When we now return to $\mathbb{R} \times S^1$ we see that the acquired space corresponds with a rag of unfolded cylinders patched together, figure 2.3. One only has to sum all the forces belonging to the straight lines from m_1 to either m_2 or one of its copies m_2' shifted by multiples of $2\pi R_C$ along the φ-axis to obtain the total gravitational force.
To make any sense this has to yield the same results as in paragraph 2.3.The total flux K spreads equally over all directions of a unit circle around m_1 and the force along a straight line then is $\frac{K}{2\pi L}$. Summed over $k \in \mathbb{Z}$ equation 2.9 is retreived. Using the same method as in paragraph 2.3.2 we recover the microscopic limit.

It is for the macroscopic limit that the usefulness of this method becomes evident. The integral extracted from the sum is an integral over the entire extra-dimensional space $\mathbb{R}^n \subset \mathbb{R}^{p+n}$. For higher dimensions with various crossover radii such an integral is much easier to calculate than n sums.
First of all we notice that all paths from m_1 to m_2 with length L have the same value for $|\vartheta|$:

$$L = \frac{x}{\cos(\vartheta)} = \sqrt{x^2 + (2\pi k)^2 R_C^2} \tag{2.13}$$

Because not every point we integrate over corresponds with a line from m_1 to m_2 we introduce the 'path density' ρ_p. This is a way to express how many paths from m_1 to m_2 there are in an area of the extra-dimensional space. Although this may depend on the coordinates in general, we will not encounter such examples and therefore view it as a constant for every space.
For $\mathbb{R} \times S^1$ there is one path from m_1 to m_2 in every interval with length $2\pi R_C$. From this we obtain:

$$\rho_p = \frac{1}{2\pi R_C} \tag{2.14}$$

To sum over all the paths from m_1 to m_2 we integrate over the n extra dimensions. Since the lengths of the paths are conserved we have to integrate the paths at the coordinates of m_2 in $\mathbb{R}^p$. For $\mathbb{R} \times S^1$ this means we have to integrate over the subset $(x, \mathbb{R}) \subset \mathbb{R}^{(1+1)}$.
We use $\vec{\tau}$ as the vector in $\mathbb{R}^n$ that points from $0 \in \mathbb{R}^n$ to a point $q \in \mathbb{R}^n$. For every $\vec{\tau}$ it is easy to calculate the value of $|\vartheta|$, so that we can express the force per straight line in terms of $\vec{\tau}$:

$$|\vartheta| = \arctan(\frac{\sqrt{\vec{\tau} \cdot \vec{\tau}}}{x})$$

We calculate the surface of the extra-dimensional space and multiply by the path density to obtain the number of paths. Every path is multiplied by the force, as defined by equation 2.5. The force is projected on the x-axis as we did in paragraph 2.3.1:

$$F_{-\hat{x}} = \int_0^\infty 2\,\mathrm{d}\|\vec{\tau}\|\ \rho_p \frac{K}{2\pi x} \cos^2(\vartheta(\vec{\tau})) = \frac{Kx}{4\pi^2 x R_C}\, 2 \int_0^{\frac{\pi}{2}} \mathrm{d}\vartheta = \frac{K}{4\pi R_C} \tag{2.15}$$

2.5 $\mathbb{R}^3 \times \left(S^1\right)^n$

In this section we will replace our toy model with one extended dimension by a more realistic model with three extended dimensions. Because we use $\mathbb{R}^3$ instead of $\mathbb{R}$ as the extended space the position vector $x \in \mathbb{R}$ is replaced by $(x, y, z) = \vec{r} \in \mathbb{R}^3$. This has two consequences. The first is that the gravitional flux is spread over $(n+3)$ dimensions. The second is that at very large scales,

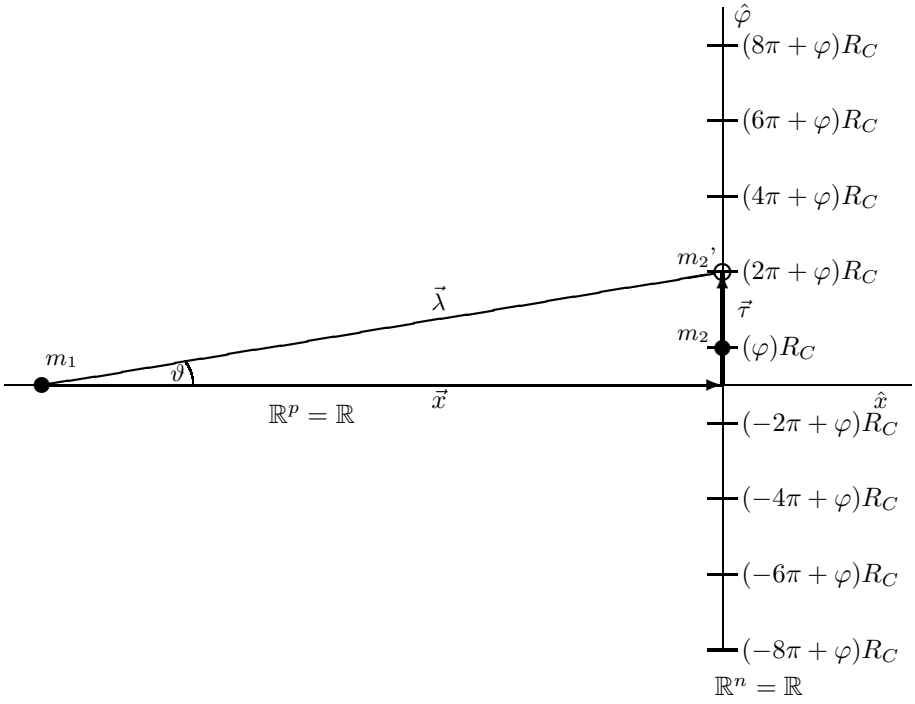

Figure 2.3: The path space for $S^1 \times \mathbb{R}$

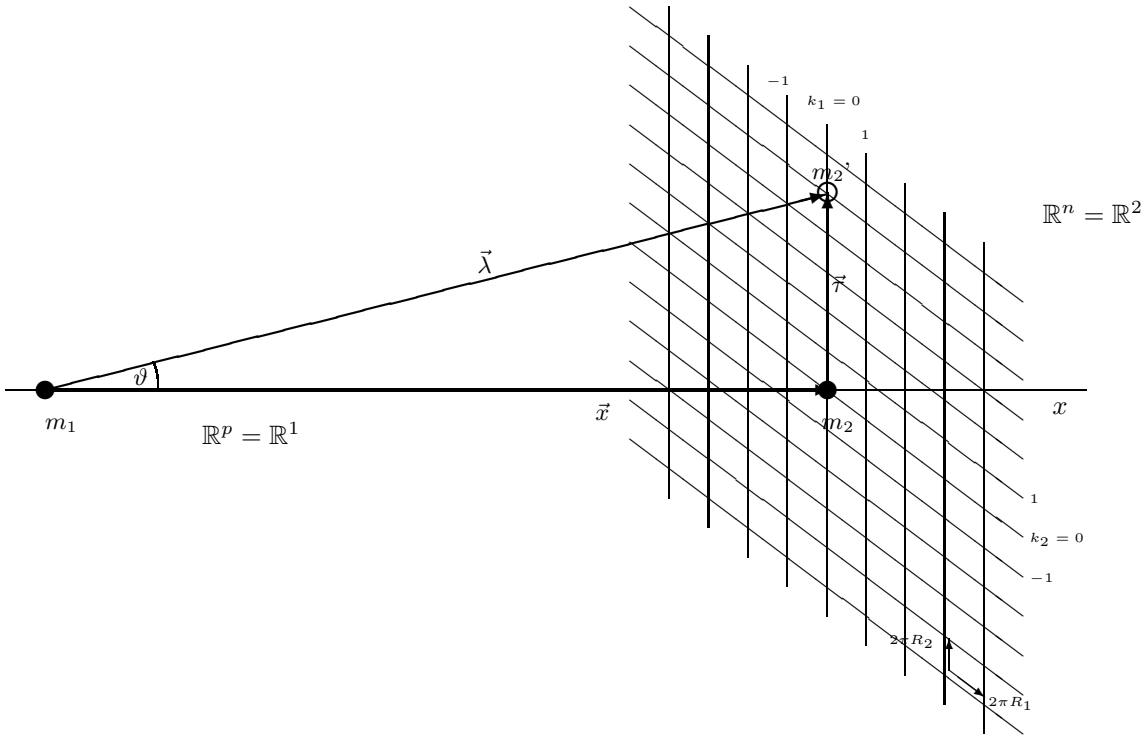

Figure 2.4: The path space for $\mathbb{R} \times S^1 \times S^1$, where m_2 is placed at $(x, 0, 0)$.

the macroscopic limit, we expect gravity to decrease with r^{-2} instead of becoming constant.
The surface the flux spreads on depends on n. To make the equations easier to understand we write the surface of a n-dimensional unit sphere as $I(n)$. At the end of the paragraph we will calculate $I(n)$. Instead of one added cylinder we now have many of them. A sensible choice of coordinates then is: $(x, y, z, \varphi_1, \ldots, \varphi_n)$. We have $k_1, \ldots, k_n$ to count the number of windings. As before we have $\varphi_i \in (-\pi, \pi]$ and $\vec{r} = (x, y, z) \in \mathbb{R}^3$. We place m_1 at $\vec{0}$ and m_2 at $(\vec{r}, \varphi_1, \ldots, \varphi_n)$.
Because the extra-dimensional space has more dimensions now we cannot account for all directions with just a plus and a minus sign for ϑ, like in paragraph 2.3. For n extra dimensions and one direction in the extended space $\vec{r}$ we need n angles to specify these vectors. We already have ϑ and we use $\alpha_1, \ldots, \alpha_{n-1}$ as the usual spherical coordinates in the extra dimensions $\mathbb{R}^n$. This defines the direction of the vector entirely. For usage we denote: $\Theta \equiv (\vartheta, \alpha_1, \ldots, \alpha_{n-1})$.
At m_1 the space is still isotropic, but now there are $(n + 3)$ dimensions for the flux to move in. The flux per straight line is $\frac{K}{I(n+3)}$. From this we can obtain the force per straight line of length L

$$F_{-\hat{\lambda}(\Theta)}(\vartheta) = \frac{\mathrm{d}\Phi}{\mathrm{d}A} = \frac{\frac{K}{I(n+3)}\mathrm{d}\Omega}{L^{n+2}\mathrm{d}\Omega} = \frac{K}{I(n+3)L^{n+2}} \quad , \tag{2.16}$$

where Ω is a solid angle in $(n + 3)$ dimensions. The flux decreases with $L^{-(n+2)}$, which is what we would expect from equation 2.3. Furthermore, notice that the direction of one term is given by:

$$-\hat{\lambda}(\Theta) = \frac{-1}{N}\left(\vec{r} + \sum_{q=1}^{n} R_q \hat{\varphi_q}\,(2\pi k_q + \varphi_q)\right) \quad , \tag{2.17}$$

where $\frac{1}{N}$ is a normalization factor.

In paragraph 2.4 we introduced the vector $\vec{\tau}$ in the extra-dimensional part $\mathbb{R}^n \subset \mathbb{R}^{(n+p)}$. Its length is

$$\|\vec{\tau}\| = \sqrt{\sum_{\zeta=1}^{n} (2\pi k_\zeta + \varphi_\zeta)^2 R_\zeta^2} \tag{2.18}$$

In general n will be larger than 1. In that case there is a sign ambiguity for ϑ, because then the extra-dimensional space contains more than two directions. Therefore we take $\vartheta \in [0, \frac{\pi}{2}]$ and define ϑ by

$$\tan(\vartheta) \equiv \frac{\|\vec{\tau}\|}{\|\vec{r}\|} \quad , \tag{2.19}$$

which means that rotation of the extra-dimensional space does not affect ϑ. If we now sum all possible paths, we obtain an expression for the total force:

$$\vec{F} = \frac{K}{I(n+3)} \sum_{k_1 \in \mathbb{Z}} \cdots \sum_{k_n \in \mathbb{Z}} \frac{-\hat{\lambda}(\Theta)}{L^{n+2}(\vec{r}, k_1, \ldots, k_n, \varphi_1, \ldots, \varphi_n)} \tag{2.20}$$

2.5.1 The macroscopic limit

If we now use the relation

$$L = \frac{\|\vec{r}\|}{\cos(\vartheta)}.$$

we find

$$F_{-\hat{r}} = \frac{K}{I(n+3)\|\vec{r}\|^{n+2}} \sum_{k_1 \in \mathbb{Z}} \cdots \sum_{k_n \in \mathbb{Z}} \cos^{n+3}(\vartheta) \tag{2.21}$$

We calculate the force in the limit $\frac{\|\vec{r}\|}{R_i} \to \infty$ for $i \in \{1, \ldots, n\}$ as described in paragraph 2.4 by using the path density

$$\rho_p = \prod_{\zeta=1}^{n} \frac{1}{2\pi R_\zeta} \quad , \tag{2.22}$$

which is the n-dimensional analogue of equation 2.14. The force per path from equation 2.16 times the path density over the entire extra-dimensional space gives:

$$F_{-\hat{r}} = \frac{K}{I(n+3)\|\vec{r}\|^{n+2}} \int_0^\infty \mathrm{d}\|\vec{\tau}\|\|\vec{\tau}\|^{n-1} I(n) \left(\prod_{\xi=1}^{n} \frac{1}{2\pi R_\xi} \right) \cos^{n+3}(\arctan(\frac{\sqrt{\sum_{\zeta=1}^{n}(2\pi k_\zeta + \varphi_\zeta)^2 R_\zeta^2}}{\|\vec{r}\|})) \quad , \tag{2.23}$$

where $\mathrm{d}\|\vec{\tau}\|\|\vec{\tau}\|^{n-1} I(n)$ is the shell of a n-dimensional sphere with a radius between $\|\vec{\tau}\|$ and $\|\vec{\tau}\| + \mathrm{d}\|\vec{\tau}\|$.
This we can further evaluate using equations 2.18 and 2.19:

$$F_{-\hat{r}} = \frac{KI(n)}{I(n+3)\|\vec{r}\|^2} \left(\prod_{\xi=1}^{n} \frac{1}{2\pi R_\xi} \right) \int_0^\infty \mathrm{d}\|\vec{\tau}\| \frac{\|\vec{\tau}\|^{n-1}}{\|\vec{r}\|^n} \cos^{n+3}(\vartheta) =$$

$$\frac{KI(n)}{I(n+3)\|\vec{r}\|^2} \left(\prod_{\xi=1}^{n} \frac{1}{2\pi R_\xi} \right) \int_0^{\frac{\pi}{2}} \mathrm{d}\vartheta \sin^{n-1}(\vartheta) \cos^2(\vartheta)$$

This can be calculated (Appendix A) and from equation A.2 we obtain:

$$F_{-\hat{r}} = \frac{KI(n)}{I(n+3)\|\vec{r}\|^2} \left(\prod_{\xi=1}^{n} \frac{1}{2\pi R_\xi} \right) \frac{(n-2)!!}{(n-1)!!} \left(1 - \frac{n}{(n+1)} \right) \cdot \begin{cases} 1 & , n \text{ even} \\ \frac{\pi}{2} & , n \text{ odd} \end{cases}$$

Here we used the definition of the double factorial $(n)!!$:

$$n!! \equiv \begin{cases} n \cdot ((n-2)!!) & n \geq 2 \\ n!! = 1 & n = 0, 1 \end{cases}$$

For $n = 1$ the $(-1)!!$ should be read as 1 to obtain the correct formula.

If there are n submillimeter dimensions we know from paragraph 2.3.1 that gravity would still fall off with r^{-2} at large scales. Furthermore, we know the force should converge to Newton's law. Using this we find for K:

$$K = \frac{G_N m_1 m_2 I(n+3)}{I(n)} \left(\prod_{\xi=1}^{n} 2\pi R_\xi \right) \frac{(n-1)!!}{(n-2)!!} \frac{n+1}{1} \cdot \begin{cases} 1 & , n \text{ even} \\ \frac{2}{\pi} & , n \text{ odd} \end{cases} \tag{2.24}$$

We can simplify this equation further if we know $I(n)$, the surface of a n-dimensional unit sphere. We can calculate it from the volume of a sphere in n dimensions:

$$V(n) = \frac{2\pi R^2}{n} V(n-2) \quad \text{with} \quad V(1) = 2R \text{ and } V(2) = \pi R^2 \quad .$$

$$I(n) = \frac{dV(n)}{dR}\Big)_{R=1}$$

From this we obtain the following equation:

$$I(n) = \begin{cases} \frac{(2\pi)^{\frac{n}{2}}}{(n-2)!!} & , n \text{ even} \\ 2\frac{(2\pi)^{\frac{n-1}{2}}}{(n-2)!!} & , n \text{ odd} \end{cases} \tag{2.25}$$

Inserting this result in equation 2.24:

$$K = 4\pi G_N m_1 m_2 \left(\prod_{\xi=1}^{n} (2\pi R_\xi) \right) \tag{2.26}$$

2.5.2 The microscopic limit

For application in the next chapter we want to know what the gravitational force is in the microscopic limit, i.e. $\frac{\|\vec{\lambda}\|}{R_\zeta} \to 0$, for all $\zeta \in \{1, \ldots, n\}$. We split $\vec{F}$ from equation 2.21 in two parts: $\vec{F}_0$ contains the term with all $k_i = 0$ and $\vec{F}_\delta$ contains all the other terms. In Appendix B is shown that we can overestimate $\|\vec{F}_\delta\|$ with equation B.1:

$$\|\vec{F}_\delta\| \leq \frac{C}{R_{min}^{n+3}} \quad ,$$

where C is a positive real constant. For the $\vec{F}_0$ term we will call such a constant D:

$$\left\|\vec{F}_0\right\| = \left\| \frac{K}{I(n+3)} \frac{-\hat{\lambda}(0)}{\|\vec{\lambda}\|^{n+2}} \right\| = \frac{D}{\|\vec{\lambda}\|^{n+3}}$$

If we now compare the two terms in the microscopic limit:

$$\lim_{\frac{\|\vec{\lambda}\|}{R_{min}} \to 0} \frac{\|\vec{F}_\delta\|}{\|\vec{F}_0\|} = 0 \quad ,$$

we see that the total contribution to the force in the microscopic limit comes from the term with all k_i zero:

$$\vec{F} = \frac{-K}{I(n+3)\|\vec{\lambda}\|^{n+2}} \hat{\lambda}(\vec{r}, \varphi_1, \ldots, \varphi_n) \tag{2.27}$$

Combining this with equation 2.26 we obtain the final expression for the force in the microscopic limit.

$$F_{-\hat{r}} = \frac{4\pi G_N m_1 m_2}{I(n+3)\|\vec{r}\|^{n+2}} \left(\prod_{\xi=1}^{n} (2\pi R_\xi) \right) \tag{2.28}$$

From this also an equation for the $(n+3)$-dimensional Newton's constant $G_N^{(n)}$ can be obtained:

$$F_{-\hat{r}} = m_1 m_2 \frac{G_N^{(n)}}{\|\vec{r}\|^{n+2}} \quad \Rightarrow \quad G_N^{(n)} = \frac{4\pi G_N}{I(n+3)} \prod_{\xi=1}^{n} (2\pi R_\xi) \tag{2.29}$$

Now we know how gravity behaves at small scales under our assumptions. For different numbers of added dimensions n and values for the crossover radii we can calculate the force, as well as the microscopic limit. In the next chapter we will study if it is possible to create microscopic black holes at the LHC using this force.

Chapter 3

Gravitational effects on the hydrogen atom

In chapter 2 we found a result for gravity in a space parametrized by the number of extra dimensions n and their crossover radii $R_1, \ldots, R_n$. Adding extra dimensions modifies the Planck length and thus the scale at which quantum gravity appears. For distances down to 10 μm direct measurements have been done. This excludes larger crossover radii. But we can do better.
Compared with the forces that are known to dominate the collisions at particle colliders, gravity is very weak. If any black hole will be made at the LHC gravity has to increase much at small scales. This increase must have some effects on a somewhat larger scale as well and that might be observable.
One of the best-known systems at relatively small scales is the hydrogen atom. Although well-described, no gravity is needed for this. This tells us that any gravitational effect on the energy levels of the electron in the hydrogen atom must be very small.
A very precisely known property of the hydrogen atom is the transition frequency of the 2S to the 1S [11]:

$$f_{2\mathrm{S}\to 1\mathrm{S}} = 2\,466\,061\,102\,474\,851 \pm 34\mathrm{Hz} \quad , \tag{3.1}$$

This value has an uncertainty of 1.4 parts in 10^{14} and improvements to decrease the relative uncertainty to several parts in 10^{18} are expected to be possible.
Theory has not yet developed to such an accurate value, but this should be possible with a lot of work. We will determine whether it would be possible with such calculations to exclude black hole production at the LHC.

3.1 Newtonian gravitation

For comparison we will calculate the correction of Newtonian gravity on the transition frequency 2S→ 1S. This we will do using time-independent perturbation theory, since the potential is time-independent. Furthermore, the potential is spherically symmetric, so we will only need the normalized radial part of the wave functions.
We write $R_{nl}(r)$ for the normalized radial wave functions of the hydrogen atom. The two wave functions we need are

$$R_{10}(r) = \frac{2}{a_0^{\frac{3}{2}}} e^{-\frac{r}{a_0}} \quad \text{and}$$

$$R_{20}(r) = \frac{1}{\sqrt{2} a_0^{\frac{3}{2}}} e^{-\frac{r}{2a_0}} \left(1 - \frac{r}{2a_0}\right) \quad . \tag{3.2}$$

The first order correction on the transition frequency then is:

$$f^{[1]}_{2\mathrm{S}\to 1\mathrm{S}} = \frac{1}{h}\langle R^{(0)}_{20}|V_G|R^{(0)}_{20}\rangle - \frac{1}{h}\langle R^{(0)}_{10}|V_G|R^{(0)}_{10}\rangle = \frac{a_0^{-3}}{h}\int_0^\infty \mathrm{d}r\; r^2 \frac{-G_N m_e m_p}{r}\frac{1}{2} e^{-\frac{r}{a_0}}\left(1 - \frac{r}{2a_0}\right)^2$$

$$-\frac{a_0^{-3}}{h}\int_0^\infty \mathrm{d}r\ r^2\left(\frac{-G_N m_e m_p}{r}\right)4e^{-\frac{2r}{a_0}} = \frac{3G_N m_e m_p}{4a_0 h} = 2.2\cdot 10^{-24}\mathrm{Hz} \quad . \tag{3.3}$$

This tells us that even the most precise measurements thinkable at this moment cannot measure effects of Newtonian gravity. Furthermore, since the term from classical gravitation is so small, we will ignore it. In the situations where this term is large compared with other terms we know that the total effect is too small to be measured.

3.2 Extra-dimensional corrections

As mentioned in paragraph 2.2 we get conservative limits if we assume that all crossover radii are the same. Therefore we will take all crossover radii to be R_C.
To calculate what the gravitational effects of the extra dimensions on the 2s→ 1s spectral line are we need a new potential. In paragraph 2.5.2 we noticed that for low momenta $F_{-\hat{r}} = \vec{F}$ and we use that now.
Since the actual expression for the gravitational force is quite complicated as we know from chapter 2, we use an approximation here. We use the microscopic limit between 0 and $10\,R_C$ as the force. We know that we cannot use the microscopic limit above R_C, but the microscopic limit decreases faster than the real force. Any effect we calculate is weaker than the actual effect, due to this approximation. Above $10\,R_C$ we use the macroscopic limit. This is a classical term. It is even smaller than equation 3.3, so we will ignore it.
From equations 2.25 and 2.28 we obtain the gravitational potential for n added dimensions:

$$V_G^{(n)} = -\frac{4\pi G_N m_e m_p}{r^{n+1}}(2\pi)^{\frac{n-3}{2}}R_C^n((n-1)!!)\begin{cases}\sqrt{\frac{\pi}{2}} & , n \text{ even}\\ 1 & , n \text{ odd}\end{cases} \tag{3.4}$$

For $n = 1$ we can calculate the correction now using equation 3.2:

$$f^{[1]}_{2\mathrm{S}\to 1\mathrm{S}} \approx \frac{1}{h}\int_0^{10R_C} r^2\,\mathrm{d}r\ R^*_{20}(r)V_G^{(1)}R_{20}(r) - \frac{1}{h}\int_0^{10R_C} r^2\,\mathrm{d}r\ R^*_{10}(r)V_G^{(1)}R_{10}(r) =$$

$$\frac{G_N m_e m_p}{a_0 h}\frac{R_C}{a_0}\left(\frac{7}{2} - 4e^{-20\frac{R_C}{a_0}} + \frac{1}{2}e^{-10\frac{R_C}{a_0}}\left(50\left(\frac{R_C}{a_0}\right)^2 - 10\frac{R_C}{a_0} + 1\right)\right)\mathrm{Hz} \tag{3.5}$$

This behaves for large R_C. The frequency correction as a function of the crossover radius $\left(\frac{R_C}{a_0}\right)$ can be found in figure 3.1 and we see that these effects are not measurable, since the values are too small. Note that $\frac{R_C}{a_0} \approx 10^6$ corresponds with $R_C \approx 50\ \mu$m, which has been excluded by direct measurements.

3.2.1 The cutoff length

For higher numbers of added dimensions n equation 3.5 will diverge, because the power of $r^{-(n+1)}$ becomes too high. However, this is no surprise. The integral diverges because we are probing classical gravity too close to our test mass m_1. We handle this by introducing two cutoff lengths.

From the theory we know that this classical expression for gravity is not valid below the Planck scale. Therefore we integrate from the cutoff length, $l_P^{(n)}$ to infinity and ignore the part between 0 and $l_P^{(n)}$, because we do not know what happens there. Notice that in this theory the Planck length depends on the number of extra dimensions and the crossover radii of these dimensions, as stated in equation 2.4.
However, it is possible that at $l_P^{(n)}$ quantum gravity should already be included. Therefore we may also use $100\,l_P^{(n)}$ as the cutoff length. Furthermore, this gives us an idea how strong the dependence on the cutoff length is. It is a way to measure the error we make. For example, a strong dependence of the results on the cutoff length implies that the obtained result is not very meaningful, since a small change in the cutoff length changes the results severely.

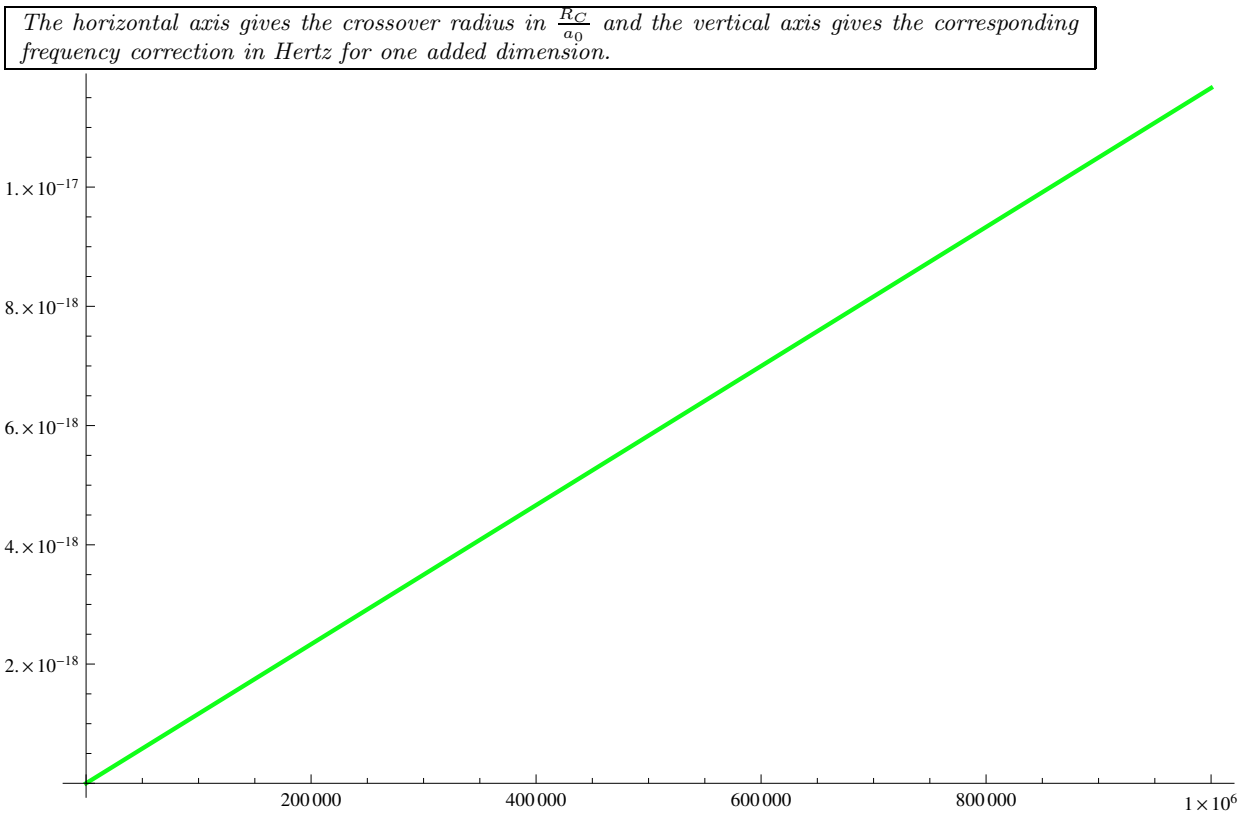

Figure 3.1: The frequency correction for one added dimension as function of the crossover radius for the 2S→ 1S transition.

Another possible cutoff can be found inside the system, because there may be a scale at which the electron and the proton are no longer spacially separated. This roughly would be the radius of the proton. There is an identifiable radius for the proton, although not very stringent, a charge radius r_{Pr}. Roughly we state that within the charge radius the quarks and the mass are contained. Again, for comparison, we like to know how strong our results depend on the cutoff length. So, we also use $10\, r_{Pr}$.

We know from paragraph 2.1 that $l_P = 1,616252 \times 10^{-35}$ m and that $l_P^{(n)}$ should be at least 10^{-19} m for the LHC to create microscopic black holes. Using this and the relation between the number of extra dimensions and the crossover radii, equations 2.4 and 2.29, we can see if these extra dimensions make the creation of microscopic black holes at the LHC possible. The results of this can be found in table 3.1. It gives the crossover radius needed for a space with n extra dimensions to make black hole creation at the LHC possible, when we use $l_P^{(n)}$ $(= 10^{-19}$ m) as our cutoff length.

3.3 Results from the transition energy

In this section we will discuss the limits on extra dimensions obtained from the integrals using the argumentation from the previous paragraphs. We want to know what possible configurations of extra-dimensional spaces may be excluded by the hydrogen atom. Anticipating upcoming im-

n	R_C	$\Delta f_{2S\to 1S}$
1	9.70×10^{10} m	1.86×10^{-2} Hz
2	6.96×10^{-5} m	3.13×10^{2} Hz
3	5.36×10^{-10} m	2.65×10^{1} Hz
4	1.40×10^{-12} m	1.24×10^{1} Hz
5	3.82×10^{-14} m	1.17×10^{1} Hz

Table 3.1: Crossover radii needed for black hole production at the LHC and the corresponding frequency corrections.

On the horizontal axis is given the number of added dimensions and on the vertical axis the smallest crossover radius that could be excluded by experiments. The grey shaded area is excluded, since the Newtonian power law has been confirmed experimentally there. The LHC *line l_{LHC} shows the smallest excluded crossover radius when no black holes are produced at the* LHC*. For different cutoff lengths the other lines give the smallest crossover radius that is excluded by the hydrogen atom.*

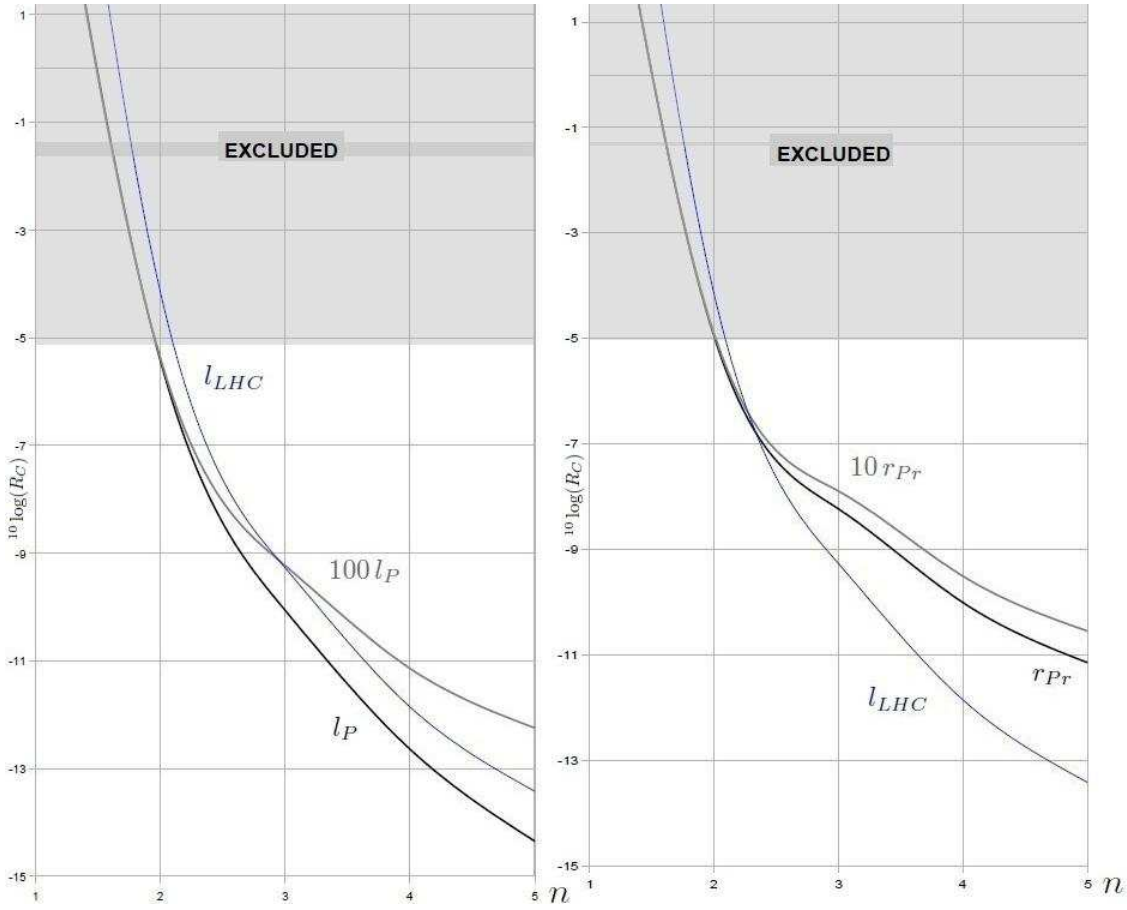

Figure 3.2: The smallest excludable values for the crossover radii for n extra dimensions using gravitational corrections of 1 Hz on the 2S→ 1S transition. The continuous line is just to guide the eye, since we do not use fractional dimensions.

provements we used a correction on the 2S→ 1S transition frequency of 1 Hz.

In the left figure of 3.2 the black line denotes the smallest excluded crossover radius for n added dimensions using $l_P^{(n)}$ as the cutoff length. Since larger crossover radii give larger corrections on the transition frequency, this must be the smallest exluded crossover radius.
When $100\,l_P$ is used instead of $l_P^{(n)}$ the grey line in the left figure of 3.2 is found. As we would expect it has higher values for R_C than the black line, since the area between $l_P^{(n)}$ and $100\,l_P^{(n)}$ is more sensitive than the other part of the integral.
In the right figure of 3.2 the same is done for the other cutoff lengths, the proton charge radius, r_{Pr} (black) and $10\,r_{Pr}$ (grey).
If experiments progress quickly enough the limit may be 10^{-3} Hz. If we used this instead of 1 Hz all crossover radii would be at least one order of magnitude smaller, which would alter the results strongly. In this case black hole creation at the LHC may be excluded by both measuring and calculating the hydrogen atom very carefully.

3.4 Implications for the LHC

The line $l_P^{(n)}$ lies entirely below l_{LHC}. This means that the Planck length is currently the only cutoff length suitable for excluding black hole creation at the LHC. So, if it is justified to use $l_P^{(n)}$ as the cutoff length precise calculations of the transition frequency $f_{2S\to 1S}$ may exclude the possibility that black holes are created at the LHC. We can see from table 3.1 that $n = 1$ is excluded by direct measurements and that for $n = 2, 3, 4, 5$ this may be done by accurately calculating and measuring the transition frequency 2S→ 1S of the hydrogen atom.
The line $100l_p$ lies partially below l_{LHC} and both the lines from the charge radius ly above the LHC-line for the interesting dimensions $3, 4$ and 5. However, for a correction on the energy of 10^{-3} Hz all lines probably may be used for certain dimensions to exclude black hole creation at the LHC and our conclusions will be much stronger, since they do not depend on the chosen cutoff length.

Chapter 4

Conclusions and Outlook

In chapter 1 of this thesis we have argued that the best known doom scenarios for the LHC do not form a threat. In chapter 2 we have worked out what Newton's gravitational law becomes in spaces with added circular dimensions and we have shown that the gravitational force increases with added dimensions. These results were applied in chapter 3 on the 1S→ 2S transition of the hydrogen atom. This we have compared with the LHC, which has led to the conclusion that black hole creation at the LHC may be excluded by improved measurements and calculations on the 1S→ 2S transition of the hydrogen atom.
We have done this under the assumption that we can only add circular dimensions to space, which is not the only possibility. There are many more ways of adding compactified dimensions and often Calabi-Yau manifolds are used for adding dimensions to space. With these manifolds more general results may be found.
Furthermore, also in our calculations we have made certain assumptions and estimates. Improvements here will give better results as well. This can be done when the actual gravitational force is used for the potential in paragraph 3.2, instead of the microscopic limit. But also finding a way to the make the results independent of the cutoff length would mean a serious improvement, since any conclusion drawn now depends heavily on the used cutoff length. This may be done by either using other models or by finding a decisive argument for a certain cutoff length.

Appendix A

Integrals

Using partial integration twice the following relation is found:

$$\int_0^{\frac{\pi}{2}} \sin^n(\vartheta)\mathrm{d}\vartheta = \left[-\frac{\sin^{n-1}(\vartheta)\cos(\vartheta)}{n}\right]_0^{\frac{\pi}{2}} + \frac{n-1}{n}\int_0^{\frac{\pi}{2}} \sin^{n-2}(\vartheta)\mathrm{d}\vartheta \quad \text{for} \quad n > 0$$

Applying the boundaries to the recursive formula yields

$$\int_0^{\frac{\pi}{2}} \sin^n(\vartheta)\mathrm{d}\vartheta = \frac{n-1}{n}\int_0^{\frac{\pi}{2}} \sin^{n-2}(\vartheta)\mathrm{d}\vartheta$$

Because of the recurrence we need to know the value for $n = 1, 2$:

$$\int_0^{\frac{\pi}{2}} \mathrm{d}\vartheta \sin(\vartheta) = 1 \qquad \int_0^{\frac{\pi}{2}} \mathrm{d}\vartheta \sin^2(\vartheta) = \frac{\pi}{4}$$

We bring the integral down to $n = 1, 2$ and end up with the following answer for $n \geq 3$:

$$\int_0^{\frac{\pi}{2}} d\vartheta \sin^n(\vartheta) = \begin{cases} \frac{\pi}{4}\prod_{\mu=1}^{\frac{1}{2}n-1}\frac{2\mu+1}{2\mu+2} & , n \text{ even} \\ \prod_{\mu=1}^{\frac{1}{2}(n-1)}\frac{2\mu}{2\mu+1} & , n \text{ odd} \end{cases} = \begin{cases} \frac{\pi}{2}\frac{(n-1)!!}{n!!} & , n \text{ even} \\ \frac{(n-1)!!}{n!!} & , n \text{ odd} \end{cases} \tag{A.1}$$

Here we used the definition of the double factorial:

$$n!! \equiv \begin{cases} n \cdot ((n-2)!!) & n \geq 2 \\ n!! = 1 & n = 0, 1 \end{cases}$$

Now we use this result to integrate the following function.

$$\int_0^{\frac{\pi}{2}} \mathrm{d}\vartheta\, \sin^{n-1}(\vartheta)\cos^2(\vartheta) = \int_0^{\frac{\pi}{2}} \mathrm{d}\vartheta \left(\sin^{n-1}(\vartheta) - \sin^{n+1}(\vartheta)\right) = \frac{(n-2)!!}{(n-1)!!}\left(1 - \frac{n}{(n+1)}\right)\cdot\begin{cases} 1 & , n \text{ even} \\ \frac{\pi}{2} & , n \text{ odd} \end{cases} \tag{A.2}$$

Appendix B

Calculating F_δ in paragraph 2.5.2

Every term in F_δ has exactly one opposite term, which means that $\Theta_i \to -\Theta_i$ for all i. Using equation 2.17 way we can write:

$$\hat{\lambda}(\Theta)+\hat{\lambda}(-\Theta)=\left(\frac{1}{N(\Theta)}+\frac{1}{N(-\Theta)}\right)\left(\vec{r}+\sum_{q=1}^{n}\varphi_q R_q\hat{\varphi_q}\right)=N(0)\left(\frac{1}{N(\Theta)}+\frac{1}{N(-\Theta)}\right)\hat{\lambda}(0) \quad ,$$

with $N(\Theta)=\sqrt{\vec{r}^2+\sum_{q=1}^{n}R_q^2\left(2\pi k_q+\varphi_q\right)^2}$ and $N(0)$ the same term with all $k_i=0$. Furthermore we can group all terms in F_δ with the same number $y=\#\{i|k_i=0\}$. Since these terms are symmetric in k_i we can rearrange and relabel the sums in such a way that we can write:

$$F_\delta=2^{n-1}\frac{-N(0)K\hat{\lambda}(0)}{I(n+3)}\sum_{y=0}^{n-1}\begin{pmatrix} n \\ y \end{pmatrix}\sum_{k_{n-y}\in\mathbb{N}}\cdots\sum_{k_1\in\mathbb{N}}\left(\frac{1}{\left(\|\vec{r}\|^2+\sum_{q=1}^{n}R_q^2\left(2\pi k_q+\varphi_q\right)^2\right)^{\frac{n+3}{2}}}+\right.$$

$$\left.\frac{1}{\left(\|\vec{r}\|^2+\sum_{q=1}^{n}R_q^2\left(-2\pi k_q+\varphi_q\right)^2\right)^{\frac{n+3}{2}}}\right) \qquad y=\#\{i|k_i=0\}$$

In the above equation $\begin{pmatrix} n \\ y \end{pmatrix}$ is the number of combinations possible to have y $k_i=0$. In this way we have only summed $2^{-(n-1)}$th part of space, so we should mutliply by 2^{n-1}, since we can treat all these parts in the same fashion. If we denote the smallest crossover radius with R_{min}:

$$F_\delta\leq\frac{-N(0)K\hat{\lambda}(0)}{R_{min}^{n+3}I(n+3)}\sum_{y=0}^{n-1}\begin{pmatrix} n \\ y \end{pmatrix}\sum_{k_{n-y}\in\mathbb{N}}\cdots\sum_{k_1\in\mathbb{N}}\frac{2}{\left(\sum_{q=1}^{n}\left(2\pi k_q-|\varphi_q|\right)^2\right)^{\frac{n+3}{2}}}$$

$$\leq\frac{-2N(0)K\hat{\lambda}(0)}{\left(2\pi R_{min}\right)^{n+3}I(n+3)}\sum_{y=0}^{n-1}\begin{pmatrix} n \\ y \end{pmatrix}\sum_{k_{n-y}\in\mathbb{N}}\cdots\sum_{k_1\in\mathbb{N}}\frac{1}{\left(\sum_{q=1}^{n}k_q^2-\frac{|\varphi_q|}{2\pi}\right)^{\frac{n+3}{2}}}\leq$$

$$\frac{-2N(0)K\hat{\lambda}(0)}{\left(2\pi R_{min}\right)^{n+3}I(n+3)}\sum_{y=0}^{n-1}\int_{\frac{1}{2}-\sqrt{\frac{|\varphi_{k_{n-y}}|}{2\pi}}}^{\infty}\mathrm{d}k_{n-y}\ldots\int_{\frac{1}{2}-\sqrt{\frac{|\varphi_{k_1}|}{2\pi}}}^{\infty}\mathrm{d}k_1\frac{1}{\left(k_1^2+\ldots+k_{n-y}^2+\sum_{b=n-y+1}^{n}\varphi_b^2\right)^{\frac{n+3}{2}}}$$

Using spherical coordinates in $n-y$ dimensions this can be shown to be finite for every y, so that we end up with the following formula:

$$\|F_\delta\|\leq\frac{C}{R_{min}^{n+3}} \qquad C\in\mathbb{R}^+ \quad , \tag{B.1}$$

in which C is the constant that comes from the integral and the constants in front of the integral.

Bibliography

[1] E.G. Adelberger, J.H. Gundlach, B.R. Heckel, S. Hoedl, and S. Schlamminger. Torsion balance experiments: A low-energy frontier of particle physics. *Progress in Particle and Nuclear Physics*, 62(1):102 – 134, 2009.

[2] Charles Alcock and Edward Farhi. Evaporation of strange matter in the early universe. *Phys. Rev. D*, 32(6):1273–1279, Sep 1985.

[3] Nima Arkani-Hamed, Savas Dimopoulos, and G. R. Dvali. The hierarchy problem and new dimensions at a millimeter. *Phys. Lett.*, B429:263–272, 1998.

[4] Arnon Dar, A. De Rujula, and Ulrich W. Heinz. Will relativistic heavy ion colliders destroy our planet? *Phys. Lett.*, B470:142–148, 1999.

[5] P.A.M. Dirac. Quantised Singularities in the Electromagnetic Field. *Proc. Roy. Soc.*, A 133:60, 1931.

[6] G. Dvali. Submillimeter Extra Dimensions and TeV-Scale Quantum Gravity. *Int. J. Th. Phys.*, 39, No 7:1717–1729, 2000.

[7] John R. Ellis, Gian Giudice, Michelangelo L. Mangano, Igor Tkachev, and Urs Wiedemann. Review of the Safety of LHC Collisions. *J. Phys.*, G35:115004, 2008.

[8] Piet Hut and Martin J. Rees. How stable is our vacuum? *Nature*, 302:508, 1983.

[9] R. L. Jaffe, W. Busza, F. Wilczek, and J. Sandweiss. Review of speculative 'disaster scenarios' at rhic. *Rev. Mod. Phys.*, 72(4):1125–1140, Oct 2000.

[10] Don N. Page. Particle emission rates from a black hole: Massless particles from an uncharged, nonrotating hole. *Phys. Rev. D*, 13(2):198–206, Jan 1976.

[11] P. Fendel M. Fischer C. Gohle M. Herrmann R. Holzwarth N. Kolachevsky Th. Udem T.W. Haensch, J. Alnis and M. Zimmermann. Precision spectroscopy of hydrogen and femtosecond laser frequency combs. *Phil. Trans. R Soc. A*, 363:2155–2163, 2005.